Int J Adv Manuf Technol (2012) 61:1–13
DOI 10.1007/s00170-011-3684-9

ORIGINAL ARTICLE

Surface roughness and chip formation in high-speed face milling AISI H13 steel

Xiaobin Cui · Jun Zhao · Chao Jia · Yonghui Zhou

Received: 6 July 2011 / Accepted: 3 October 2011 / Published online: 22 October 2011

Abstract Many previous researches on high-speed machining have been conducted to pursue high machining efficiency and accuracy. In the present study, the characteristics of cutting forces, surface roughness, and chip formation obtained in high and ultra high-speed face milling of AISI H13 steel (46–47 HRC) are experimentally investigated. It is found that the ultra high cutting speed of 1,400 m/min can be considered as a critical value, at which relatively low mechanical load, good surface finish, and high machining efficiency are expected to arise at the same time. When the cutting speed adopted is below 1,400 m/min, the contribution order of the cutting parameters for surface roughness Ra is axial depth of cut, cutting speed, and feed rate. As the cutting speed surpasses 1,400 m/min, the order is cutting speed, feed rate, and axial depth of cut. The developing trend of the surface roughness obtained at different cutting speeds can be estimated by means of observing the variation of the chip shape and chip color. It is concluded that when low feed rate, low axial depth of cut, and cutting speed below 1,400 m/min are adopted, surface roughness Ra of the whole machined surface remains below 0.3 μm, while cutting speed above 1,400 m/min should be avoided even if the feed rate and axial depth of cut are low.

Keywords Cutting forces · Surface roughness · Chip formation · High-speed face milling · AISI H13 steel

X. Cui · J. Zhao (✉) · C. Jia · Y. Zhou
Key Laboratory of High Efficiency and Clean Mechanical Manufacture of MOE, School of Mechanical Engineering, Shandong University,
Jinan 250061, People's Republic of China
e-mail: zhaojun@sdu.edu.cn

1 Introduction

The primary objective of manufacturing operation is to efficiently produce parts with high quality. The high-speed machining processes can produce more accurate parts as well as reduce the costs associated with assembly and fixture storage by allowing several process procedures to be combined into a monolithic one [1]. For the purpose of enhancing machining efficiency and accuracy at the same time, many significant researches on high-speed machining have been conducted.

High-speed milling has been widely used in the manufacturing of aluminum aeronautical and automotive components so as to generate surfaces with high geometric accuracy. The tool materials and rigid machine tools have advanced to be applied in hard milling, which can even be an alternative for the grinding process to some extent [2, 3]. In order to reveal the effects of cutting conditions especially cutting speed on the machining efficiency and product quality in high-speed hard milling, comprehensive and thorough researches on surface roughness and chip formation should be conducted.

There are relatively few researches relating to surface roughness in the field of high-speed milling of hardened steels, and studies on chip formation are scant. As is stated by Ghani et al. [4], when high cutting speed, low feed rate, and low depth of cut were adopted, good surface finish can be obtained in semifinish and finish machining hardened AISI H13 steel using TiN-coated carbide insert tools. The effects of cutting parameters on surface roughness in high-speed side milling of hardened die steels were investigated by Vivancos et al. [5, 6], and mathematical models of surface roughness were established by means of the design of experiment (DOE) method. Toh [7] investigated and evaluated the different cutter path orientations when high-

speed finish milling hardened steel, and the results demonstrated that vertical upward orientation is generally preferred in terms of workpiece surface roughness. Ding et al. [8] experimentally investigated the effects of cutting parameters on cutting forces and surface roughness in hard milling of AISI H13 steel with coated carbide tools. And empirical models for cutting forces and surface roughness were established. The analysis results showed that finish hard milling can be an alternative to grinding process in the die and mold industry. Siller et al. [9] studied the impact of a special carbide tool design on the process viability of the face milling of hardened AISI D3 steel in terms of surface quality and tool life. It was found that surface roughness Ra values from 0.1 to 0.3 μm can be obtained in the workpiece with an acceptable level of tool life.

Previous studies provide much valuable information for the understanding of surface roughness in high-speed hard milling. But very few researches were conducted to investigate the surface roughness in high-speed face milling of hardened steel. And probably due to the relatively small tool diameter and the high hardness of the workpiece, the upper limits of the cutting speed in these studies mentioned above are much lower than those (1,100 m/min) in the researches on tool wear in high-speed face milling of hardened AISI 1045 steel [1].

Because of the great high-temperature strength and wear resistance, AISI H13 tool steel is widely applied in extrusion, hot forging, and pressure die casting. In the present study, characteristics of cutting forces, surface roughness, and chip formation obtained under different cutting speeds in high and ultra high-speed face milling of AISI H13 steel (46–47 HRC) are identified and compared. For the purpose of experimental investigating the effects of cutting parameters especially cutting speed on surface roughness, Taguchi method was used for the DOE. Because of the dynamic effects, runout, vagaries of the table feed, and back cutting in the milling process, the profile of the milled surface can vary substantially in either the feed or perpendicular directions. Wilkinson [10] pointed out that, although some profiles were measured in nonback cutting regions, it still seems that such variations were realistic. In the present study, for the purpose of reducing such variation, the milled surface is divided into four regions, and those regions are investigated separately and integratedly.

2 Experimental procedures

2.1 Workpiece material

A block of AISI H13 steel hardened to 46 to 47 HRC was used in the present study. The nominal chemical composition of the H13 tool steel under consideration is shown in Table 1. Dimensions of the block were designed so as to avoid back cutting as shown in Fig. 1.

2.2 Cutting tool and machining center

A Seco R220.53-0125-09-8C tool holder with a tool diameter of 125 mm, major cutting edge angle of 45°, cutting rake angle of 10°, axial rake angle of 20°, and radial rake angle of −5° was used in the milling tests. The tool holder is capable of carrying eight inserts. The tungsten carbide insert SEEX 09T3AFTN-D09, which is coated with Ti(C, N)–Al_2O_3, was used in the experiments. In order to simplify the analysis, only one of the teeth was used in all the milling tests. All of the surfaces were milled using fresh cutting edges. The milling tests were conducted on a vertical CNC machining center DAEWOO ACE-V500 with a maximum spindle rotational speed of 10,000 rpm and a 15-kW drive motor without cutting fluid.

2.3 Cutting tests

As has been mentioned, it has been found that the use of high cutting speed, low feed rate, and low depth of cut leads to a good surface finish in semifinish and finish machining hardened AISI H13 steel [4]. Therefore, for the purpose of acquiring better surface finish at high cutting speed (upper limit 2,400 m/min), low feed rate (0.02–0.06 mm/tooth) and low axial depth of cut (0.1–0.3 mm) were adopted in the milling tests. Symmetric milling was applied, and the radial depth of cut was fixed as 75 mm as shown in Fig. 1. In all the milling tests, the feed length was set to be invariable 112.5 mm so that back cutting can be avoided.

The effects of cutting speed on cutting forces, surface roughness Ra, and chip formation are focused on in the present study. Firstly, experiments with all the cutting parameters fixed except for the cutting speed v ranging from 200 to 2,400 m/min with 200 m/min as an interval were performed. Axial depth of cut a_p and feed rate f_z were set to be invariable 0.2 mm and 0.04 mm/tooth, respectively.

The Taguchi method uses a special design of orthogonal arrays to study the entire parameters space with only a small number of experiments [11]. After the experiments with cutting speed in the range from 200 to 2,400 m/min, in order to distinguish the differences of the effects of cutting parameters on surface roughness obtained within different cutting speed ranges, two L_9 orthogonal arrays, each of which has four columns and nine rows, were used in the present study. For both of the orthogonal arrays, the three influencing factors were cutting speed, feed rate, and axial depth of cut, and one

Table 1 Nominal chemical composition of AISI H13 tool steel (in weight percent)

C	Mn	Si	Cr	Mo	V	Ni	Fe
0.32–0.45	0.20–0.50	0.80–1.2	4.75–5.50	1.10–1.75	0.80–1.20	0–0.30	Bal

column of array was left empty for the error of experiments. Table 2 shows the three levels of the factors in the two arrays. The experimental layouts ME_1 and ME_2 are shown in Tables 3 and 4.

The machined surface of the workpiece material was divided into four regions as shown in Fig. 2. And the total machined surface is represented by R_5. In region R_2 the entrance and exit angles stay the same, while in the other regions those angles keep changing. Moreover, for any small time period, the milling conditions in regions R_1 and R_2 can still be considered as symmetric milling, but in regions R_3 and R_4 they seemed to be two different kinds of asymmetric milling. It is inferred that these differences will lead to varying characteristics of the mechanical and thermal loads when machining different regions, and finally affect the way how the surfaces generate. Taking these into consideration, in each test for each region denoted in Fig. 2, surface roughness Ra was measured three times along the feed direction.

Under given milling conditions, each test was replicated three times. The surface roughness Ra in different regions was measured along the feed direction using a portable surface roughness tester (Model TR200, China). The sampling length and number of spans were set to be 0.8 mm and five, respectively. As shown in Fig. 3, the cutting forces were measured using Kistler piezoelectric dynamometer (type 9257B) mounted on the machine table. And the charge generated at the dynamometer was amplified by means of a multichannel charge amplifier (type 5070A). The sampling frequency of data was set as 7,000 Hz. After the experiments the tool wear was examined with an optical microscope and the chips were observed using a Keyence VHX-600E 3D digital microscope with a large depth of field.

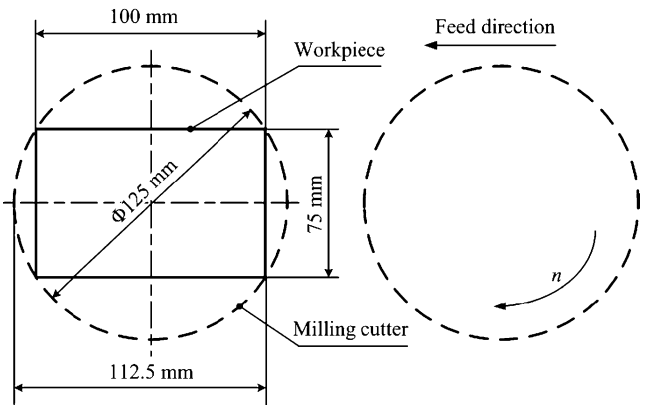

Fig. 1 The setup of face milling

3 Results and discussion

3.1 Cutting force

The effects of cutting speed on cutting forces are focused on in the present study. In the milling tests with cutting speed ranging from 200 to 2,400 m/min, the cutting force signatures were picked at the time when the milling cutter reached the midpoint of region R_2. For per cutting force component, there were 7,000 data points in each recorded signature. The data point F_m of the resultant cutting force is calculated from the cutting force components as shown in Eq. 1:

$$F_m = \sqrt{(F_{xm})^2 + (F_{ym})^2 + (F_{zm})^2} \tag{1}$$

where F_{xm}, F_{ym}, and F_{zm} are corresponding data points of the cutting force components in x, y, and z directions, respectively. Due to the continuous variability of the sampled data, the static force component F_{sta} can be defined as the mean value of the sampled data point F_m [12] as shown in Eq. 2:

$$F_{sta} = \frac{1}{N}\left(\sum_{m=1}^{N} F_m\right) \tag{2}$$

where N is the number of the data points. Based on the research by Toh [13], the dynamic cutting force F_{dyn} can be calculated as shown in Eq. 3:

$$F_{dyn} = F_{max} - F_{sta} \tag{3}$$

where F_{max} is the maximum data value of all the data points of the resultant cutting force.

Since each test was replicated three times, for each cutting speed, there exist three values for F_{sta} and F_{dyn}, respectively. Figures 4 and 5 show the developing trends of the average values of the static cutting force and the dynamic cutting force with the cutting speed, respectively. It can be seen from Fig. 4 that as the cutting speed increases, the static cutting force firstly increases approaching a peak value at a cutting speed of 1,000 m/min and then begin to decrease. At the cutting speed of 1,400 m/min, the static cutting force reaches a valley value. When the cutting

Table 2 Factors and selected levels in the face milling experiments

Factor	Cutting parameter	Unit	Level 1	Level 2	Level 3
A	Cutting speed (v_1)	m/min	350	700	1,050
B	Cutting speed (v_2)	m/min	1,400	1,750	2,100
C	Feed rate (f_z)	mm/tooth	0.02	0.04	0.06
D	Depth of cut (a_p)	mm	0.10	0.20	0.30

speed increases over 1,400 m/min, the static cutting force keeps increasing.

When the cutting speed is relatively low, the cutting temperature is low and adhesion is less likely to happen between the tool and the workpiece material. Adhesion peaks at some intermediate temperature [14]. When the cutting speed is below 1,000 m/min, the cutting temperature increases with the cutting speed, leading to the more serious adhesion. It is inferred that, mainly due to the increase of the friction coefficient induced by serious adhesion, the static cutting force increases. As the cutting speed increases over 1,000 m/min, higher cutting temperature occurred. At high cutting temperature, adhesion is reduced as thermal softening has greater effect on the interface or on the workpiece material [14]. Higher cutting temperature arises in the shear zone, leading to the reduction of the yield strength of the workpiece material, chip thickness, and tool chip contact area. Moreover, the increase of cutting temperature results in the decrease of the friction coefficient between the tool rake face and the chip. And the shear angle will increase. Finally the static cutting force will decrease. When the cutting speed surpasses 1,400 m/min, the tool wear increases greatly with the cutting speed as shown in Fig. 7. Because of the high plowing forces induced by the increased contact area of the larger flank wear face of the cutter acting on the workpiece, the static cutting force increases with the cutting speed when the cutting speed is above 1,400 m/min.

Figure 5 shows that when the cutting speed increases, the dynamic cutting force keeps increasing until it reaches a peak value at about 1,000 m/min. Then it decreases until the cutting speed is 1,400 m/min. As the cutting speed surpasses 1,400 m/min, the dynamic cutting force will increase. It seems that the developing trends of the static and dynamic cutting forces are similar. This can be attributed to the profound effect of the static cutting force on the occurrence of cutter vibration. Since the tool wear increases rapidly with the cutting speed when the cutting speed is above 1,400 m/min as shown in Fig. 7, it is inferred that besides the effects of the fixturing elements and the machine tool system, the higher tool wear also has great contribution to the increasing trend of the dynamic cutting force when the cutting speed increases over 1,400 m/min. The evolution of the dynamic cutting force with the cutting speed indicate that for the cutting parameters under consideration, relatively stable cutting condition can still be obtained at a high cutting speed of 1,400 m/min. The relatively stable cutting condition is beneficial to the surface finish of the workpiece. It is concluded that the cutting speed of 1,400 m/min can be considered as a critical value for both of the static and dynamic cutting forces.

3.2 Surface roughness

Figure 6 shows the surface roughness in different regions vs. cutting speed v. The surface roughness y_i in region R_i is calculated by means of the following equation:

$$y_i = \frac{1}{n}\left(\sum_{j=1}^{n} y_{ij}\right) \tag{4}$$

where n is the number of repeated test, namely three; y_{ij} is the average value of Ra in region R_i at the jth test (i=1, 2,

Table 3 Experimental layout ME_1 using an L_9 orthogonal array

Exp. no.	A (v_1)	C (f_z)	D (a_p)	E (error)
1	1	1	1	
2	1	2	2	
3	1	3	3	
4	2	1	2	
5	2	2	3	
6	2	3	1	
7	3	1	3	
8	3	2	1	
9	3	3	2	

Table 4 Experimental layout ME_2 using an L_9 orthogonal array

Exp. no.	B (v_2)	C (f_z)	D (a_p)	F (error)
10	1	1	1	
11	1	2	2	
12	1	3	3	
13	2	1	2	
14	2	2	3	
15	2	3	1	
16	3	1	3	
17	3	2	1	
18	3	3	2	

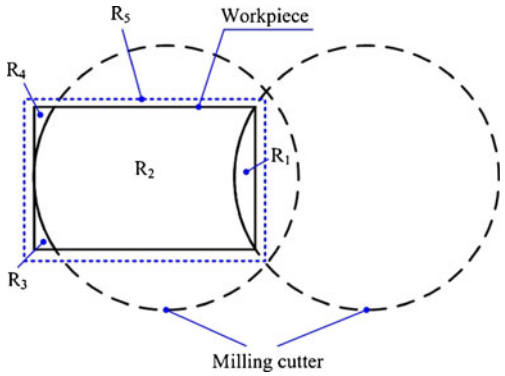

Fig. 2 Division of the machined surface

3, 4, 5; j=1, 2, 3). The average surface roughness y_{5j} of the total machined surface is determined by Eq. 5:

$$y_{5j} = y_{1j}S_1/S_5 + y_{2j}S_2/S_5 + y_{3j}S_3/S_5 + y_{4j}S_4/S_5 \quad (5)$$

where S_k is the area of the region R_k (k=1, 2, 3, 4, 5).

It can be seen from Fig. 6 that the curves (solid line) of the surface roughness in regions R_1 and R_2 with cutting velocity are similar, while those in region R_3 and R_4 are similar. For surface roughness in all the regions, cutting speed v=800 m/min is the optimum one, and v=1,400 m/min can be considered as a transition value above which the surface roughness in the five regions increase rapidly. It must be pointed that when the cutting speed v is at a rather high value of 1,400 m/min, as for the total machined surface R_5 good surface quality (0.068 μm) can still be obtained.

Though the machined surface has been divided into four regions and each test was replicated three times, for the surface roughness in each region, there still seems to be some randomness. In order to reveal the developing trends of surface roughness in a more clear way, the curves of the surface roughness with the cutting speed are fitted as shown in Fig. 6 (dotted line). It can be seen from these fitted curves that as the cutting velocity increases, the surface roughness in different regions all exhibit similar developing trend: they

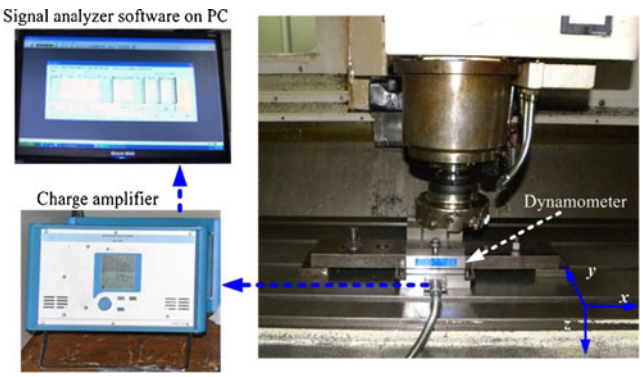

Fig. 3 Photos of the experimental setup

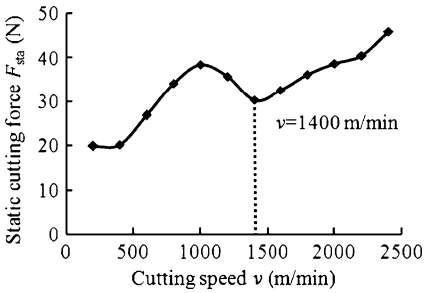

Fig. 4 Static cutting force F_{sta} vs. cutting speed v (f_z=0.04 mm/tooth, a_p=0.2 mm)

all decrease firstly and then increase. Equations 6, 7, 8, 9, and 10 are the fitted formulas for the surface roughness in regions R_1, R_2, R_3, R_4, and R_5, respectively.

$$y_1 = 1.29 \cdot 10^{-7}v^2 - 2.25 \cdot 10^{-4}v + 1.27 \cdot 10^{-1}(\mu m) \quad (6)$$

$$y_2 = 8.68 \cdot 10^{-8}v^2 - 1.06 \cdot 10^{-4}v + 8.51 \cdot 10^{-2}(\mu m) \quad (7)$$

$$y_3 = 1.18 \cdot 10^{-7}v^2 - 2 \cdot 10^{-4}v + 1.65 \cdot 10^{-1}(\mu m) \quad (8)$$

$$y_4 = 8.13 \cdot 10^{-8}v^2 - 1.36 \cdot 10^{-4}v + 1.21 \cdot 10^{-1}(\mu m) \quad (9)$$

$$y_5 = 9.08 \cdot 10^{-8}v^2 - 1.18 \cdot 10^{-4}v + 9.07 \cdot 10^{-2}(\mu m) \quad (10)$$

The R squares (the coefficient of multiple determination, measuring how successful the fit is in explaining the variation of the data) for the five formulas are 0.92, 0.93, 0.91, 0.89, and 0.95, respectively. According to the fitted formulas, for different regions, the cutting speeds at which the optimum surface quality can be obtained are between 600 and 900 m/min. The surface quality is expected to be optimal when the cutting speed adopted is in this speed range.

Since both the cutting forces and the surface roughness are low at an ultra high cutting speed of 1,400 m/min,

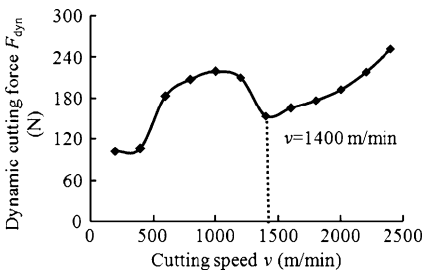

Fig. 5 Dynamic cutting force F_{dyn} vs. cutting speed v (f_z=0.04 mm/tooth, a_p=0.2 mm)

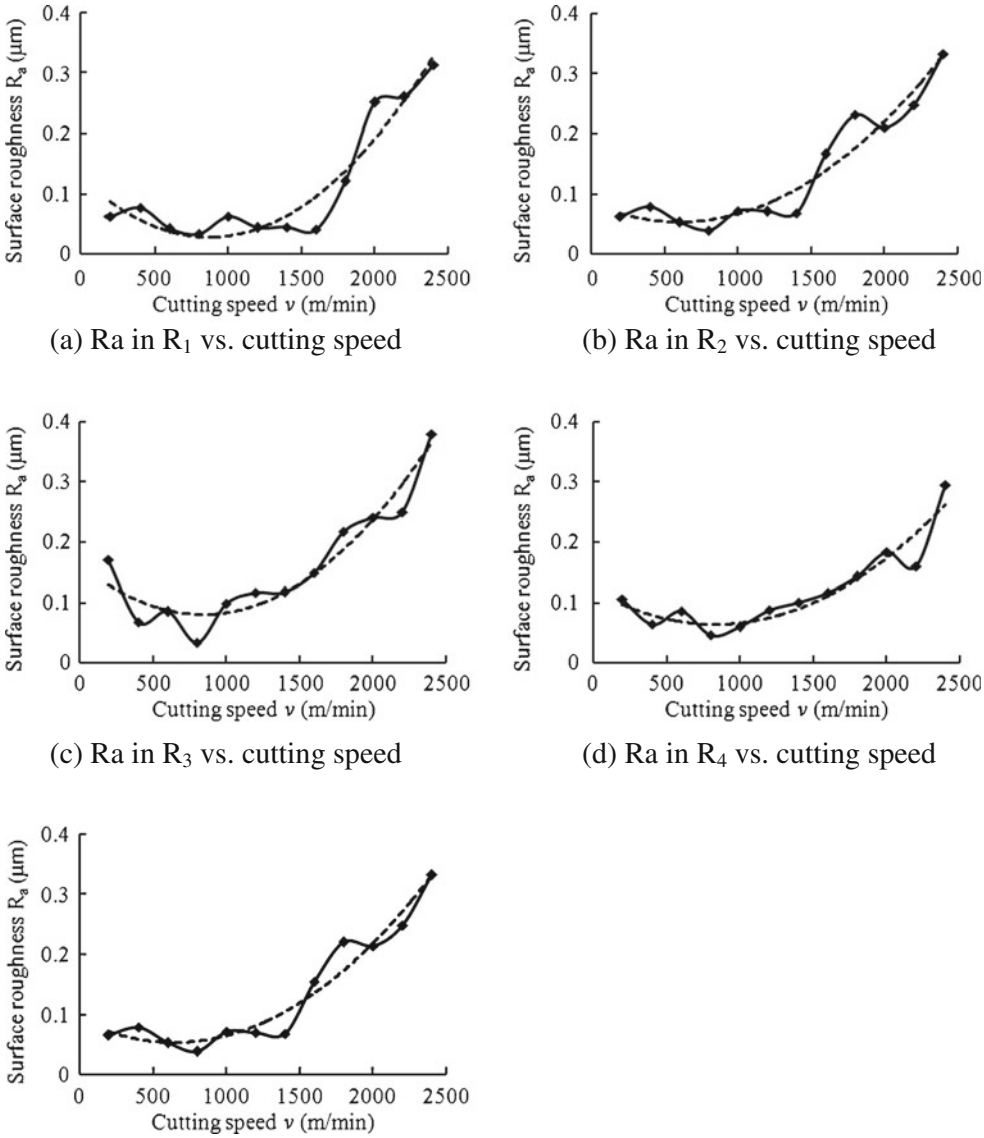

(a) Ra in R_1 vs. cutting speed

(b) Ra in R_2 vs. cutting speed

(c) Ra in R_3 vs. cutting speed

(d) Ra in R_4 vs. cutting speed

(e) Ra in R_5 vs. cutting speed

Fig. 6 Surface roughness Ra in different regions vs. cutting speed v (f_z=0.04 mm/tooth, a_p= 0.2 mm). **a** Ra in R_1 vs. cutting speed. **b** Ra in R_2 vs. cutting speed. **c** Ra in R_3 vs. cutting speed. **d** Ra in R_4 vs. cutting speed. **e** Ra in R_5 vs. cutting speed

relatively low mechanical load, good surface quality, and high machining efficiency are expected to arise at the same time for the cutting parameters under consideration. Though the machining efficiency is a little lower, cutting speeds below 1,400 m/min can still be used to obtain good surface finish, but the cutting speeds above 1,400 m/min should be avoided.

Figure 7 shows the evolution of the average flank wear VB after one pass of the workpiece surface with the cutting speed. It can be seen that when the cutting speed is below 1,400 m/min, the tool wear rate is relatively small. As the cutting speed surpasses 1,400 m/min, the tool wear rate increases rapidly with the cutting speed. Taking the developing trend of the surface roughness with cutting speed into consideration, it is inferred that when the cutting speed is below 1,400 m/min, the effect of tool wear on surface roughness is small. But as the cutting speed surpasses 1,400 m/min, the higher tool wear rate contributes greatly to the increase of the surface roughness with the cutting speed.

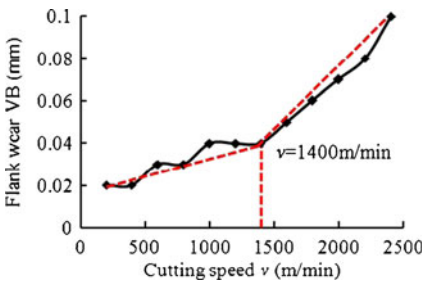

Fig. 7 Flank wear of the cutting tool after one pass of the workpiece surface vs. cutting speed v (f_z=0.04 mm/tooth, a_p=0.2 mm)

As 1,400 m/min is a transition cutting speed for surface roughness, two experimental layouts ME_1 and ME_2 are designed to investigate the effects of cutting parameters on surface roughness within two different cutting speed ranges, namely <1,400 and ≥1,400 m/min, as shown in Tables 3 and 4. The results of surface roughness show that for all the regions surface roughness Ra remains below 0.3 μm can be obtained using the cutting parameter combinations listed in the experimental layout ME_1. Surface roughness below 0.3 μm is an acceptable value for the comparison with other finishing process like grinding [15], while the surface roughness Ra obtained under some cutting parameter combinations with relatively higher cutting speeds in ME_2 is much larger than 0.3 μm.

The signal to noise (*S*/*N*) ratio used in the Taguchi method reflects both the average and the variation of the quality characteristics. Therefore, in the present study, instead of the average value, the *S*/*N* ratio is used so as to convert the trial result data into a value for the evaluation characteristics in the optimum setting analysis. The *S*/*N* ratio η_i for region R_i can be expressed in decibel units, and it is defined by a logarithmic function based on the mean square deviation around the target:

$$\eta_i = -10log\left[\frac{1}{n}\left(\sum_{j=1}^{n} {y_{ij}}^2\right)\right] \tag{11}$$

where all the symbols have the same meaning as they did in Eq. 4. It can be seen from Eq. 11 that the larger is the *S*/*N* ratio, the smaller is the variance of surface roughness Ra around the desired value.

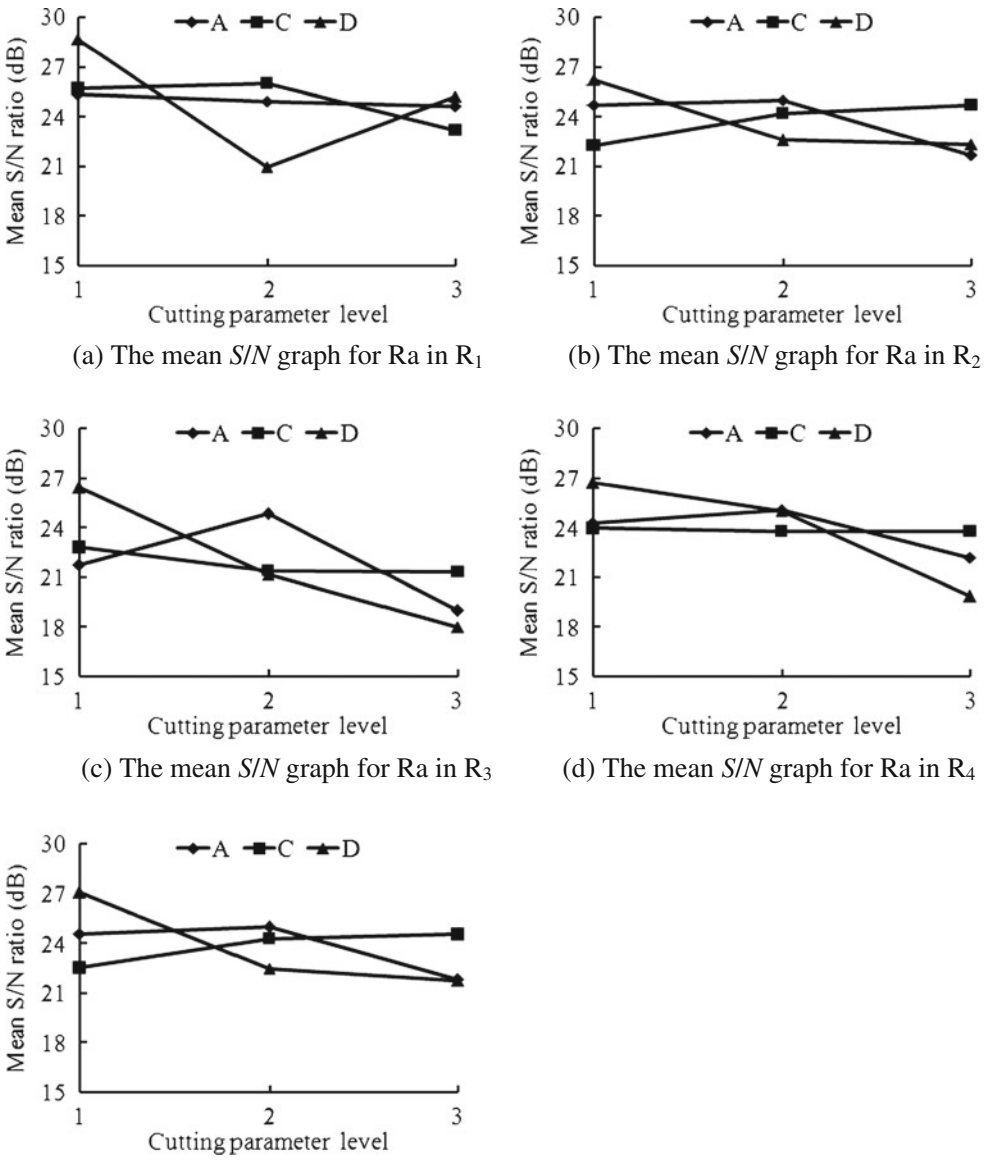

(a) The mean *S*/*N* graph for Ra in R_1 (b) The mean *S*/*N* graph for Ra in R_2

(c) The mean *S*/*N* graph for Ra in R_3 (d) The mean *S*/*N* graph for Ra in R_4

(e) The mean *S*/*N* graph for Ra in R_5

Fig. 8 The mean *S*/*N* graph for surface roughness in different regions (ME_1). **a** The mean *S*/*N* graph for Ra in R_1. **b** The mean *S*/*N* graph for Ra in R_2. **c** The mean *S*/*N* graph for Ra in R_3. **d** The mean *S*/*N* graph for Ra in R_4. **e** The mean *S*/*N* graph for Ra in R_5

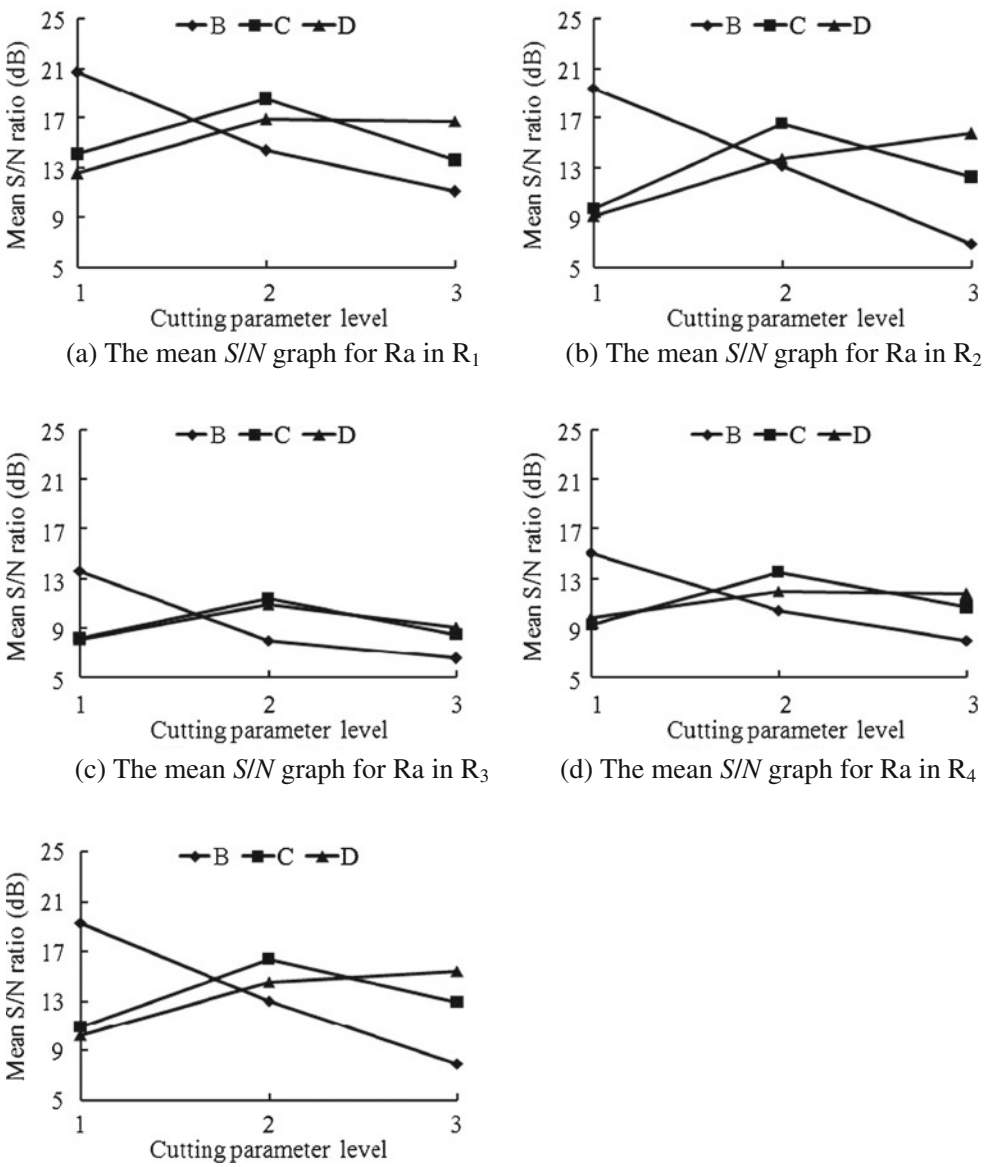

(a) The mean *S/N* graph for Ra in R_1

(b) The mean *S/N* graph for Ra in R_2

(c) The mean *S/N* graph for Ra in R_3

(d) The mean *S/N* graph for Ra in R_4

(e) The mean *S/N* graph for Ra in R_5

Fig. 9 The mean *S/N* graph for surface roughness in different regions (ME_2). **a** The mean *S/N* graph for Ra in R_1. **b** The mean *S/N* graph for Ra in R_2. **c** The mean *S/N* graph for Ra in R_3. **d** The mean *S/N* graph for Ra in R_4. **e** The mean *S/N* graph for Ra in R_5

Table 5 The cutting parameters and corresponding *S/N* ratios for Ra in R_5 (ME_1)

Exp. no.	v_1 (m/min)	f_z (mm/tooth)	a_p (mm)	*S/N* ratio
1	350	0.02	0.1	26.97
2	350	0.04	0.2	23.80
3	350	0.06	0.3	22.97
4	700	0.02	0.2	22.04
5	700	0.04	0.3	23.85
6	700	0.06	0.1	29.03
7	1,050	0.02	0.3	18.52
8	1,050	0.04	0.1	25.24
9	1,050	0.06	0.2	21.61

Table 6 The cutting parameters and corresponding *S/N* ratios for Ra in R_5 (ME_2)

Exp. no.	v_2 (m/min)	f_z (mm/tooth)	a_p (mm)	*S/N* ratio
10	1,400	0.02	0.1	12.88
11	1,400	0.04	0.2	23.85
12	1,400	0.06	0.3	21.18
13	1,750	0.02	0.2	12.00
14	1,750	0.04	0.3	17.39
15	1,750	0.06	0.1	9.78
16	2,100	0.02	0.3	7.85
17	2,100	0.04	0.1	8.12
18	2,100	0.06	0.2	7.98

Table 7 Results of the ANOVA for Ra in the total machined surface R_5 (ME_1)

Source	*df*	Sum of squares	Variance	*F* value	Contribution (%)
A	2	18.08	9.04	22.60	22.76
C	2	7.34	3.67	9.18	8.62
D	2	49.77	24.89	62.23	64.46
Error	2	0.79	0.40		4.16
Total	8	75.98			100

Figures 8 and 9 show the mean *S*/*N* response graphs for surface roughness Ra in different regions. It can be seen that, generally all the mean *S*/*N* ratios in Fig. 8 are much higher than those in Fig. 9, indicating that if the cutting speed surpasses 1,400 m/min, the surface quality will deteriorate badly. From Fig. 8 which shows the mean *S*/*N* graph for ME_1, it can be seen that the feed rate f_z has little effect on the surface roughness in the five regions. As for region R_1, the effect of cutting speed v on surface roughness is little. However, for all the other four regions, as the cutting speed increases, the surface roughness decrease firstly and then increase. In region R_1, as the depth of cut a_p increases, the surface roughness increase firstly and then decrease, while in the other regions the surface roughness increase with the depth of cut. It can be seen from the mean *S*/*N* graph for ME_2 in Fig. 9 that the surface roughness in the five regions all increases with the cutting speed *v*. As the feed rate f_z increases, the surface roughness in all the regions decreases firstly and then increases. The surface roughness in all the five regions except for region R_3 decrease with the depth of cut a_p. In region R_3, as the depth of cut increases, the surface roughness decreases firstly and then increases. It can be concluded that within different speed ranges, the effects of the cutting parameters on surface roughness in the five regions change greatly.

For the experimental layout ME_1, the optimum combinations of the cutting parameter levels are A1C2D1, A2C3D1, A2C1D1, A2C1D1, and A2C3D1 for surface roughness in regions R_1, R_2, R_3, R_4, and R_5, respectively. As for the experimental layout ME_2, the optimum combinations of the cutting parameter levels are B1C2D2, B1C2D3, B1C2D2, B1C2D2, and B1C2D3. The optimum combinations of the cutting parameter levels for surface roughness in regions R_3 and R_4 are the same. And it seems that low feed rate and low depth of cut is beneficial especially for surface roughness in these two regions. It can be concluded that because of the varying characteristics of the mechanical and thermal loads, for different regions, there definitely exist differences in the formation of surface profiles.

Tables 5 and 6 show the cutting parameters and corresponding *S*/*N* ratios for the total machined surface R_5 obtained by means of Eqs. 4 and 5. Based on the results listed in Tables 5 and 6, the results of analysis of variance (ANOVA) for surface roughness in the total machined surface can be obtained as shown in Tables 7 and 8. For the experimental layout ME_1, the contribution order of the cutting parameters for surface roughness Ra is axial depth of cut, cutting speed, and feed rate, and the contribution of feed rate is very small. As for ME_2, the order is cutting speed, feed rate and axial depth of cut, and the contributions of feed rate and axial depth of cut are approximately the same. It can be concluded that as the cutting speed surpasses 1,400 m/min, the degree of influences of cutting speed and feed rate on surface roughness Ra increases substantially especially for cutting speed, while that of axial depth of cut decreases substantially.

The surface roughness Ra in the total machined surface R_5 is focused on in the regression analysis. The form of the Taylor's tool life equation in metal cutting is used, and a functional relationship between the average value of surface roughness in region R_5 and the cutting parameters could be postulated by:

$$\mathrm{Ra} = a v^b f_z^c a_p^d (\mu\mathrm{m}) \tag{12}$$

Table 8 Results of the ANOVA for Ra in the total machined surface R_5 (ME_2)

Source	*df*	Sum of squares	Variance	*F* value	Contribution (%)
B	2	192.90	96.45	87.68	65.98
C	2	47.08	23.54	21.40	15.53
D	2	46.85	23.43	21.30	15.45
Error	2	2.20	1.10		3.04
Total	8	289.03			100

By means of a logarithmic transformation, the nonlinear form of Eq. 12 can be converted into the following linear form:

$$\ln \mathrm{Ra} = \ln a + b \ln v + c \ln f_z + d \ln a_p \tag{13}$$

where a, b, c, and d are the corresponding parameters. After regression analysis, the regression equations for the surface roughness are obtained as follows:

$$\mathrm{Ra}(\mathrm{ME}_1) = 0.0176 \times v^{0.2582} \times f_z^{-0.1896} \times a_p^{0.5757} (\mu\mathrm{m}) \tag{14}$$

$$\mathrm{Ra}(\mathrm{ME}_2) = 3.9432 \times 10^{-13} \times v^{3.3612} \times f_z^{-0.3223} \times a_p^{-0.5207} (\mu\mathrm{m}) \tag{15}$$

where $\mathrm{Ra}(\mathrm{ME}_1)$ and $\mathrm{Ra}(\mathrm{ME}_2)$ represent the surface roughness in experimental layouts ME_1 and ME_2, respectively.

Figure 10 compares the fitted values of surface roughness and the observed values for ME_1 and ME_2. Figure 11 shows the relative percentage error between the fitted and the observed values. The average value of the relative error for $\mathrm{Ra}(\mathrm{ME}_1)$ and $\mathrm{Ra}(\mathrm{ME}_2)$ are 4.6921% and 4.8906%, respectively. It can be concluded that Eqs. 14 and 15 can describe the behavior of the data well.

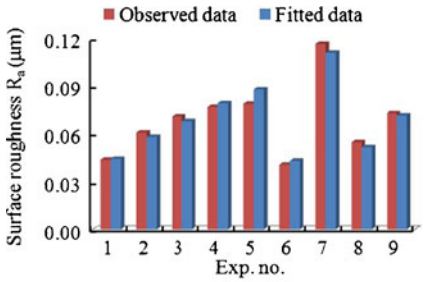

(a) The fitted and observed surface roughness in ME_1.

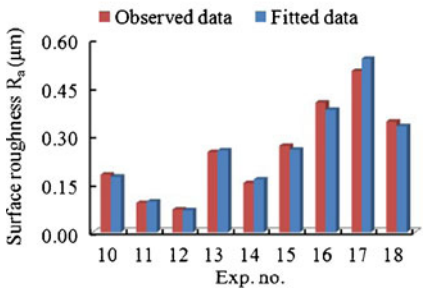

(b) The fitted and observed surface roughness in ME_2.

Fig. 10 The fitted values of surface roughness vs. the observed values. **a** The fitted and observed surface roughness in ME_1. **b** The fitted and observed surface roughness in ME_2

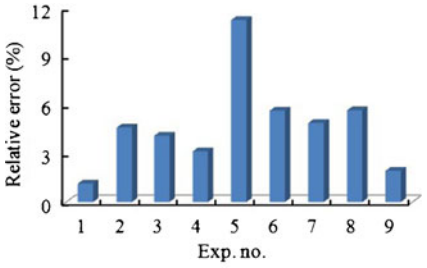

(a) Deviation of the fitted surface roughness Ra (ME_1).

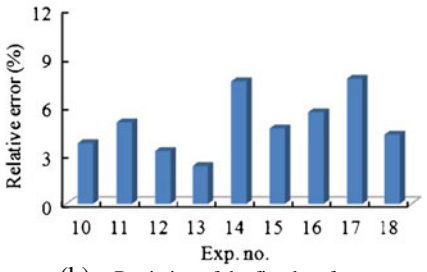

(b) Deviation of the fitted surface roughness Ra (ME_2).

Fig. 11 Deviation of the fitted surface roughness from the observed values. **a** Deviation of the fitted surface roughness Ra (ME_1). **b** Deviation of the fitted surface roughness Ra (ME_2)

3.3 Chip formation

Figure 12 shows the chip formation under different cutting speeds with axial depth of cut a_p and feed rate f_z fixed as 0.2 mm and 0.04 mm/tooth, respectively. As the cutting speed increases, both the shape and the color of the chip change gradually. When the cutting speed increases, the shape of the chip changes in the following order: washer-shaped chip (v=200 m/min), wave-shaped chip (v=400 m/min), arc-shaped chip (v=600 m/min), long strip of chip (v=800–1,400 m/min), short strip of chip (v=1,600–2,200 m/min), and powder-shaped chip (v=2,400 m/min). It is found that the color of the chip is blue when the cutting velocity is relatively low (v=200–600 m/min). At higher cutting speed (v=800–1,200 m/min), the color turns into purple. When the cutting speed is no less than 1,400 m/min, the chip color is yellow.

At the cutting speed of 800 m/min, the chip color turns from blue into purple and the shape of the chip changes from arc-shaped chip to long strip of chip. As has been discussed, at this cutting speed, optimum surface quality can be obtained as shown in Fig. 6. When the cutting speed surpasses 1,400 m/min, short strip of chip is about to form and the chip color changes into yellow. This cutting speed can be seen as a transition cutting speed for surface roughness as has been mentioned. It seems that the correspondence between the chip formation and the surface roughness is obvious, indicating that the evolution of the

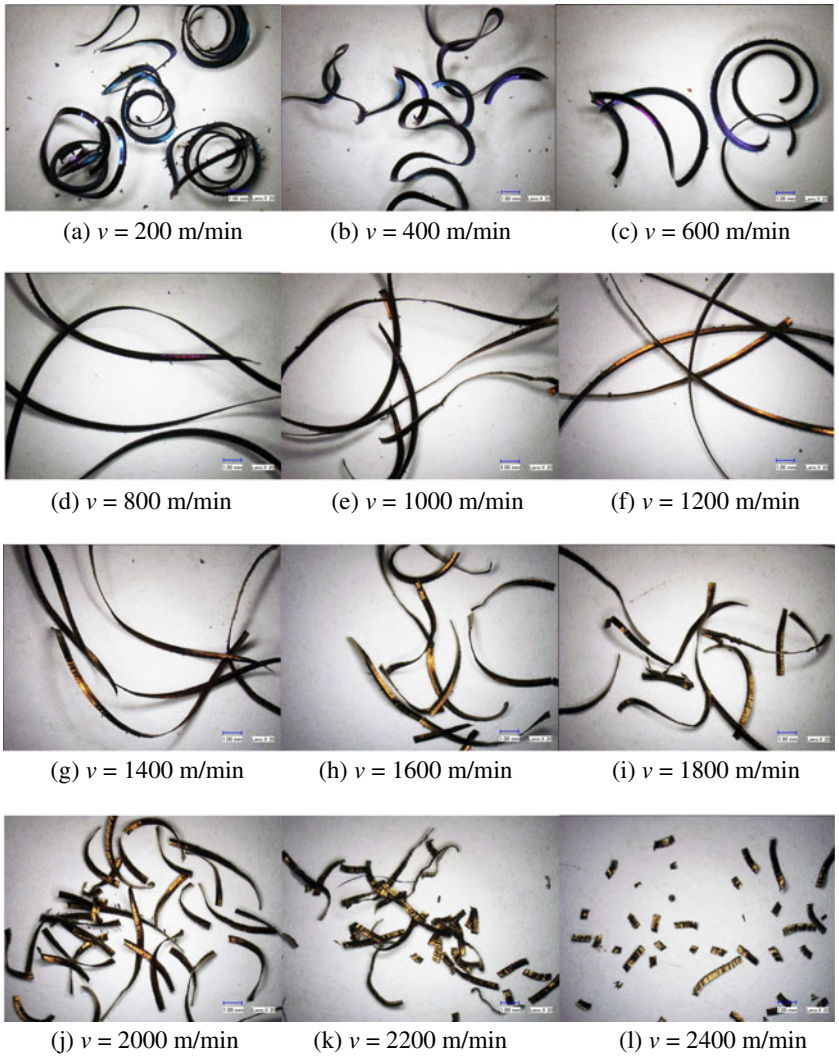

Fig. 12 Chip formation under different cutting speeds (f_z=0.04 mm/tooth, a_p=0.2 mm). **a** v=200 m/min. **b** v=400 m/min. **c** v=600 m/min. **d** v=800 m/min. **e** v=1,000 m/min. **f** v=1,200 m/min. **g** v=1,400 m/min. **h** v=1,600 m/min. **i** v=1,800 m/min. **j** v=2,000 m/min. **k** v=2,200 m/min. **l** v=2,400 m/min

surface quality can be estimated by means of observing the variation of the chip shape and color.

It is also found that the serrated chip begins to arise when the cutting speed is about 400 m/min as shown in Fig. 13b. As the cutting speed increases, the serrated chip becomes more and more obvious. As shown in Fig. 13e at the cutting speed of 2,400 m/min, the serrated chip is about to be separated.

4 Conclusions

The effects of cutting speed on cutting forces, surface roughness, and chip formation in high and ultra high-speed face milling of AISI H13 steel were focused on in the present study. Taking the critical cutting speed 1,400 m/min into consideration, the effects of cutting parameters on surface roughness within two cutting speed ranges (<1,400 and ≥1,400 m/min) were investigated experimentally by means of Taguchi method. In order to reduce the undesirable variations of surface roughness, back cutting was avoided, and the milled surface was divided and investigated separately and integratedly. The following conclusions can be obtained:

- When the cutting speed increases from 200 to 2,400 m/min with feed rate f_z and axial depth of cut a_p fixed, both the static and dynamic cutting forces reach a valley value at a cutting speed of 1,400 m/min. It can be concluded that relatively stable cutting condition which is beneficial to the surface finish of the workpiece can still be obtained at a high cutting speed of 1,400 m/min.
- As the cutting speed increases from 200 to 2,400 m/min with feed rate f_z and axial depth of cut a_p fixed as 0.04 mm/tooth and 0.2 mm, the surface roughness in different regions all decreases firstly and then increases. The cutting speed of 1,400 m/min is considered as a critical value above which the surface roughness will deteriorate badly. When the cutting speed is between 600

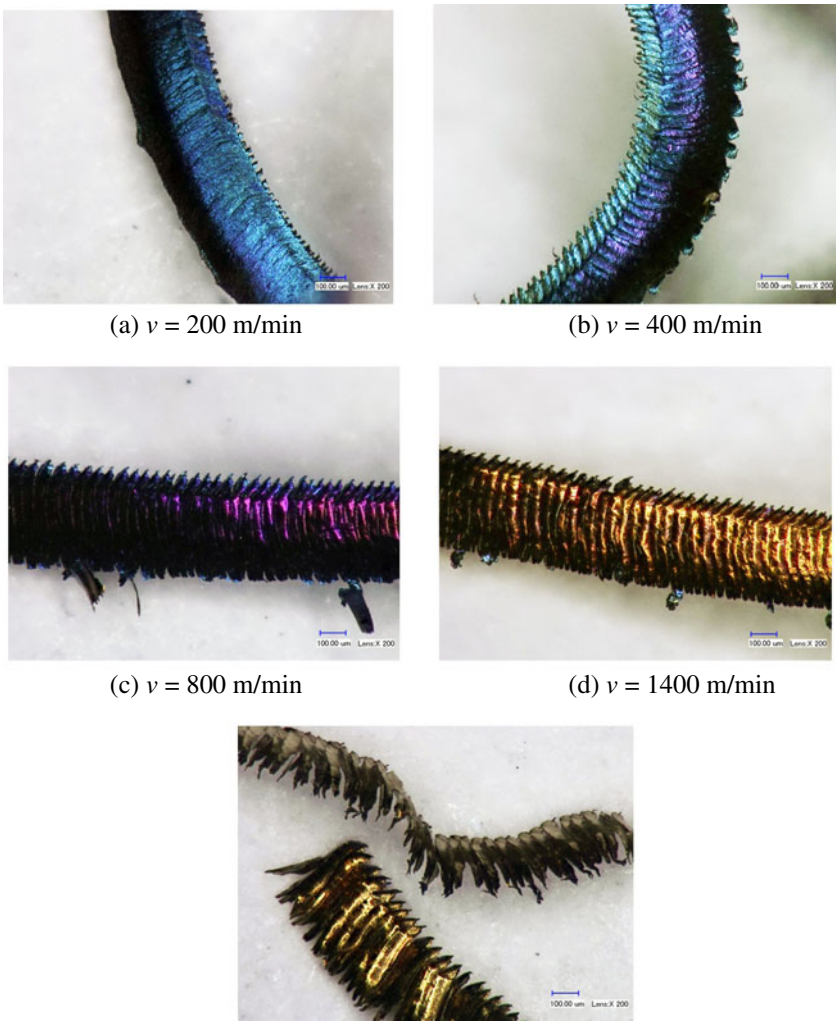

(a) v = 200 m/min (b) v = 400 m/min

(c) v = 800 m/min (d) v = 1400 m/min

(e) v = 2400 m/min

Fig. 13 Magnified chip formation under different cutting speeds (f_z=0.04 mm/tooth, a_p=0.2 mm) **a** v=200 m/min. **b** v=400 m/min. **c** v=800 m/min. **d** v=1,400 m/min. **e** v=2,400 m/min

and 900 m/min, low surface roughness is expected to be obtained. When the cutting speed surpasses 1,400 m/min, the higher tool wear rate has great effect on the increase of the surface roughness with the cutting speed. One thousand four hundred meters per minute is considered to be a critical cutting speed for both the cutting forces and surface roughness. At the cutting speed of 1,400 m/min good surface quality, relatively low mechanical load and high machining efficiency are expected to arise at the same time for the cutting parameters under consideration.

- Due to the variations of the characteristics of the mechanical and thermal loads, the surface roughness Ra in different regions of the machined surface respond in varying ways to the changes of cutting parameters. For the experimental layouts ME_1 and ME_2, the optimum combinations of the cutting parameter levels for surface roughness in the whole machined surface R_5 are A2C3D1 (v=700 m/min, f_z=0.06 mm/tooth, a_p=0.1 mm) and B1C2D3 (v=1,400 m/min, f_z=0.04 mm/tooth, a_p=0.3 mm). The results of ANOVA for surface roughness of the total machined surface show that for the experimental layout ME_1, the contribution order of the cutting parameters is axial depth of cut, cutting speed, and feed rate, and the contribution of feed rate is very little; while for ME_2, the order is cutting speed, feed rate, and axial depth of cut, and the contributions of feed rate and axial depth of cut are roughly the same. When the cutting speed surpasses 1,400 m/min, the cutting speed and feed rate become much more influential to the surface roughness especially for cutting speed, while the effect of axial depth of cut declines greatly. It is found that when the cutting speed is below 1,400 m/min, low surface roughness Ra below 0.3 μm can be obtained. By means of regression analysis, two equations for the surface roughness of the total machined surface R_5 in experimental layouts ME_1 and ME_2 are fitted. It is found that those equations can describe the behavior of the data well.
- As the cutting speed changes from 200 to 2,400 m/min with invariable feed rate f_z 0.04 mm/tooth and axial

depth of cut a_p 0.2 mm, both the shape and color of the chip change gradually. There exists obvious correspondence between the shape, color of the chip, and the surface roughness obtained at different cutting speeds. When the cutting speed surpasses 1,400 m/min which is considered as a transition speed below which good surface finish can still be obtained, short strip of chip is about to form and the color of the chip turns into yellow. It seems that the evolution of the surface quality with cutting speed can be estimated by means of observing the variation of the chip formation.

Acknowledgments This research is supported by the National Basic Research Program of China (2009CB724402), the National Natural Science Foundation of China (51175310), and the Graduate Independent Innovation Foundation of Shandong University, GIIFSDU (yzc10119).

References

1. Liu ZQ, Ai X, Zhang H, Wang ZT, Wan Y (2002) Wear patterns and mechanisms of cutting tools in high-speed face milling. J Mater Process Technol 129:222–226
2. Nelson S, Schueller JK, Tlusty J (1998) Tool wear in milling hardened die steel. J Manuf Sci Eng 120(4):669–673
3. Iqbal A, He N, Li L, Dar NU (2007) A fuzzy expert system for optimizing parameters and predicting performance measures in hard-milling process. Expert Syst Appl 32(4):1020–1027
4. Ghani JA, Choudhury IA, Hassan HH (2004) Application of Taguchi method in the optimization of end milling parameters. J Mater Process Technol 145(1):84–92
5. Vivancos J, Luis CJ, Costa L (2004) Optimal machining parameters selection in high speed milling of hardened steels for injection moulds. J Mater Process Technol 155–156:1505–1512
6. Vivancos J, Luis CJ, Ortiz JA (2005) Analysis of factors affecting the high-speed side milling of hardened die steels. J Mater Process Technol 162–163:696–701
7. Toh CK (2006) Cutter path orientations when high-speed finish milling inclined hardened steel. Int J Adv Manuf Technol 27:473–480
8. Ding TC, Zhang S, Wang YW, Zhu XL (2010) Empirical models and optimal cutting parameters for cutting forces and surface roughness in hard milling of AISI H13 steel. Int J Adv Manuf Technol 51:45–55
9. Siller HR, Vila C, Rodríguez CA, Abellán JV (2009) Study of face milling of hardened AISI D3 steel with a special design of carbide tools. Int J Adv Manuf Technol 40:12–25
10. Wilkinson P, Reuben RL, Jones JDC, Barton JS, Hand DP, Carolan TA, Kidd SR (1997) Surface finish parameters as diagnostics of tool wear in face milling. Wear 205:47–54
11. Yang WH, Tarng TS (1998) Design optimization of cutting parameters for turning operations based on the Taguchi method. J Mater Process Technol 84:122–129
12. Dimla DE, Lister PM (2000) On-line metal cutting tool condition monitoring. I: force and vibration analysis. Int J Mach Tools Manuf 40(5):739–768
13. Toh CK (2004) Static and dynamic cutting force analysis when high speed rough milling hardened steel. Mater Des 25:41–50
14. Childs T, Maekawa K, Obikawa T, Yamane Y (2000) Metal machining: theory and applications. Wiley, New York
15. Boothroyd G, Knight WA (2005) Fundamentals of machining and machine tools, 3rd edn. CRC, New York